

# Indian summer monsoon simulations with CFSv2: a microphysics perspective

Hemantkumar S. Chaudhari<sup>1</sup> · Anupam Hazra<sup>1</sup> · Subodh K. Saha<sup>1</sup> · Ashish Dhakate<sup>1</sup> · Samir Pokhrel<sup>1</sup>

Received: 27 February 2015 / Accepted: 14 May 2015 / Published online: 23 May 2015  
© Springer-Verlag Wien 2015

**Abstract** The present study explores the impact of two different microphysical parameterization schemes (i.e. Zhao and Carr, *Mon Wea Rev* 125:1931–1953, 1997: called as ZC; Ferrier, *Amer Meteor Soc* 280–283, 2002: called as BF) of National Centers for Environmental Prediction (NCEP) Climate Forecast System version 2 (CFSv2) on Indian summer monsoon (ISM). Critical relative humidity (RHcrit) plays a crucial role for the realistic cloud formation in a general circulation model (GCM). Hence, impact of RHcrit along with microphysical scheme on ISM is evaluated in the study. Model performance is evaluated in terms of simulation of rainfall, lower and upper tropospheric circulations, cloud fraction, cloud condensate and outgoing longwave radiation (OLR). Climatological mean features of rainfall are better represented by all the sensitivity experiments. Overall, ZC schemes show relatively better rainfall patterns as compared to BF schemes. BF schemes along with 95 % RHcrit (called as BF95) show excess precipitable water over Indian Ocean basin region, which seems to be unrealistic. Lower and upper tropospheric features are well simulated in all the sensitivity experiments; however, upper tropospheric wind patterns are underestimated as compared to observation. Spatial pattern and vertical profile of cloud condensate is relatively better represented by ZC schemes as compared to BF schemes. Relatively more (less) cloud condensate at upper level has lead to relatively better (low) high cloud fraction in ZC (BF) simulation. It is seen that OLR in ZC simulation have great proximity with observation. ZC (BF) simulations depict low

(high) OLR which indicates stronger (weaker) convection during ISM period. It implies strong (weak) convection having stronger (weaker) updrafts in ZC (BF). Relatively more (less) cloud condensate at upper level of ZC (BF) may produce strong (weak) latent heating which may lead to relatively strong (weak) convection during ISM. The interaction among microphysics, thermodynamics, and dynamics works in tandem through a closed feedback loop.

## 1 Introduction

Indian summer monsoon is an important facet of life in India (e.g., Webster et al. 1998; Kripalani et al. 2003). The variable nature of Indian summer monsoon rainfall (ISMR) has a profound impact on socioeconomic growth. About 80 % of the annual rainfall over India occurs during the summer monsoon period (June–September). Monsoon is a large-scale phenomenon, and it is linked with different global circulation systems. The role of cloud properties on Indian summer monsoon (ISM) is not well understood. The understanding of water content, formation of cloud hydrometeors, latent heating, and a combination of microphysical and dynamical processes during ISM is essential (Hazra et al. 2013a, b). The importance of interaction of cloud properties and dynamics in governing the ISM variability (Hazra et al. 2013a; Kumar et al. 2014), and thus, improvement of their biases in the model is crucial for the better ISM rainfall prediction. Rainfall variability is also governed by clouds which play a leading role in radiative energy and water cycle balances (Stephens et al. 2002; Hazra et al. 2014). Linkage between cloud and microphysical processes is well known. Clouds play a crucial role in the dynamics and thermodynamics of the atmosphere. The realistic representation of cloud formation by general circulation model (GCM) is one of the major

✉ Hemantkumar S. Chaudhari  
hemantkumar@tropmet.res.in

<sup>1</sup> Indian Institute of Tropical Meteorology, Dr. Homi Bhabha Road, NCL Post, Pashan, Pune 411 008, India

attributions to the improved depiction of ISMR. In the tropics, the upper level clouds containing ice and mixed phases significantly affect the radiation balance of the atmosphere (Baker 1997). GCM experiments have also pinpointed that the microphysical and dynamical processes of clouds influence the radiative processes (e.g., Arakawa and Schubert 1974). Thus, the treatment of clouds which is the product of complicated interaction among radiation, moist convective process with large-scale circulation and microphysical processes, is one of the most complex tasks in GCM. Ice and mixed-phase clouds are important part of the climate systems and yet poorly understood and represented in GCMs to simulate the climate (Waliser et al. 2009). A high degree of uncertainty still remains in observations of even bulk ice properties (Waliser et al. 2009). Therefore, quantitative forecasting of precipitation has been one of the major challenges in operational GCM. The effects of clouds on the treatment of condensation and evaporation are also important in the precipitation calculation. Although reasonable precipitation forecasts have been produced using simple schemes, one cannot neglect cloud water and cloud ice in the model thermodynamic and hydrological fields. Furthermore, the exclusion of ice-phase clouds in the model can lead to underestimation of latent heat release below the freezing level ( $<0$  °C) and therefore weakens the feedback of condensation to the thermodynamic fields. Recently, Waliser et al. (2009) have shown that the representation of cloud ice in GCM is inadequate. So, this is an ongoing challenge to rectify these shortcomings and to reduce the model bias in the cloud hydrometeor production. Previous studies based on observations have pinpointed that microphysical properties are associated with monsoon (e.g., Rajeevan et al. 2013; Hazra et al. 2015a; De et al. 2015). In this perspective, the parameterization of microphysics has utmost importance in GCMs for the simulation of ISM. It has motivated us to take up the present study which evaluates impact of microphysical schemes on ISM by utilization of fully coupled ocean–atmosphere model.

Recent generation dynamical coupled ocean–atmosphere systems of National Centers for Environmental Prediction (NCEP) Climate Forecast System (CFS) version 2 (hereafter referred as CFSv2, Saha et al. 2014a) have played a vital role in betterment of tropical seasonal prediction (e.g., Saha et al. 2014b; Saha et al. 2013; Pokhrel et al. 2012; Hazra et al. 2015b). CFSv2 has two types of microphysical schemes namely Zhao and Carr (1997) and Ferrier et al. (2002). Details of the clouds schemes are presented in section 2.2. For better elucidation of cloud processes, we have also performed sensitivity experiments using different RHcrit values (90 and 95 %) for the present CFSv2 microphysical scheme of Zhao and Carr (1997) and Ferrier et al. (2002). In general, RHcrit is empirically adjusted within the cloud cover formulation to mimic the observation or to fine-tune the

climatological simulations. Impact of RHcrit along with microphysical scheme on ISM is also evaluated in this study.

This paper is arranged as follows: Section 2 deals with model description and design of numerical experiments. Section 3 illustrates results and discussion. Conclusions are stated in section 4 of the manuscript.

## 2 Model description and design of numerical experiment

### 2.1 Model description

NCEP has developed the Climate Forecast System version 2 (CFSv2; Saha et al. 2010, 2014a) fully coupled ocean–atmosphere–land model with advanced physics, increased resolution, and refined initialization to improve the seasonal climate forecasts. CFSv2 consists of a spectral atmospheric model at a resolution of T126 ( $\sim 0.937^\circ$ ) with 64 hybrid vertical levels and the Geophysical Fluid Dynamics Laboratory (GFDL) Modular Ocean Model, version 4p0d (Griffies et al. 2004) at  $0.25\text{--}0.5^\circ$  grid spacing with 40 vertical layers. The atmosphere and ocean models are coupled with no flux adjustment. It utilizes simplified Arakawa–Schubert (SAS) cumulus convection (Hong and Pan 1998) with momentum mixing. It implements orographic gravity wave drag based on Kim and Arakawa (1995) approach and subgrid scale mountain blocking by Lott and Miller (1997). It uses rapid radiative transfer model (RRTM) shortwave radiation with maximum random cloud overlap (Iacono et al. 2000; Clough et al. 2005). It is also coupled to a four-layer Noah land surface model (Ek et al. 2003) and a two-layer sea ice model (Wu et al. 2005).

### 2.2 Cloud microphysics scheme in CFSv2

There are two microphysical schemes in CFSv2 namely Zhao and Carr (1997) and Ferrier et al. (2002) implemented by Moorthi et al. (2001) and Nakagawa et al. (2011). The conversion of precipitation is diagnostically calculated directly from the cloud water/cloud ice mixing ratio, and precipitation rate is parameterized following Zhao and Carr (1997) for ice and Sundqvist et al. (1989) for liquid water. The convective source term is provided by the cloud top detrainment in the convective parameterization (Moorthi et al. 2001, 2010). The large-scale condensation is based on Zhao and Carr (1997) and Sundqvist et al. (1989). Moorthi et al. (2001) introduced a simple cloud microphysics parameterization (Zhao and Carr 1997; Sundqvist et al. 1989) in CFSv2 where cloud condensate is a prognostic variable. Both large-scale condensation and the detrainment of cloud water from cumulus convection provide sources of cloud condensate (Moorthi et al. 2010; Sun et al. 2010).

On the other hand, the Ferrier cloud microphysics scheme used in the NCEP North American Mesoscale Forecast System (Ferrier et al. 2002) was tested for the NCEP Global Forecast System (GFS) and consequently implemented in CFSv2 (Moorthi et al. 2001; Nakagawa et al. 2011). The Ferrier scheme is a double-moment bulk cloud microphysics scheme which predicts various forms of condensate in the form of cloud water, small ice crystals, rain, and precipitation ice. Precipitation ice is determined to be in the form of snow, graupel, or sleet (frozen raindrops) based on the density of the precipitation ice, which is explicitly calculated. Ferrier scheme is designed for the use in high-resolution model and does not consider partial cloud explicitly. Ferrier scheme is applied separately to the cloudy and clear with precipitation portion of the grid.

For calculating cloud optical thickness, all the cloud condensate in a grid box is assumed to be in the cloudy region. So, the cloud condensate mixing ratio is computed by the ratio of grid mean condensate mixing ratio and cloud fraction when the latter is greater than zero (Saha et al. 2014a). The fractional cloud cover used in the radiation calculation is diagnostically determined from the predicted cloud condensate based on the approach of Xu and Randall (1996).

### 2.3 Design of numerical experiment

The CFSv2 has been ported on IBM Prithvi High Performance Computing (HPC) system at Indian Institute of Tropical Meteorology (IITM), Pune. According to Sundqvist et al. (1989), relative humidity-based cloud schemes assume cloud formation after the relative humidity (RH) reaches a critical value (RHcrit). In general, RHcrit is empirically adjusted within the cloud cover formulation to mimic the observation or to adjust the long-term climatological simulations (Walcek 1994). This tuning of RHcrit within a physically plausible range gives a better representation of cloud processes and also produces a better resemblance with observation (Slingo et al. 1987; Sanderson et al. 2010).

Cloud scheme in CFSv2 is also based on relative humidity. For the same, four sets of sensitivity experiments are performed by specifying different values of RHcrit (low and high values) along with microphysical scheme. The details of experimental design are as follows:

ZC90 run: Zhao and Carr (1997) microphysical scheme + value of RHcrit is set as 90, 90, and 90 % for low, mid, and high levels, respectively.

BF90 run: Ferrier et al. (2002), Moorthi et al. (2001) microphysical scheme + value of RHcrit is set as 90, 90, and 90 % for low, mid, and high levels, respectively.

ZC95 run: Zhao and Carr (1997) microphysical scheme + value of RHcrit is set as 95, 95, and 95 % for low, mid, and high levels, respectively.

BF95 run: Ferrier et al. (2002), Moorthi et al. (2001) microphysical scheme + value of RHcrit is set as 95, 95, and 95 % for low, mid, and high levels, respectively.

Initial conditions for the atmosphere and the ocean are taken from NCEP Climate Forecast System Reanalysis (CFSR, Saha et al. 2010). In the present experiments, the CFSv2 has been integrated for 10 years. In our analysis, we have utilized the last 9 years of simulations after excluding the first model year for spin-up purpose. Climatological mean of required fields are presented in these analyses and compared with observation and reanalysis products. The biases (model minus observation) of various variables (precipitation, cloud fraction, outgoing longwave radiation, temperature, precipitable water) are also computed.

### 2.4 Observed datasets used

This study uses rainfall datasets from the Global Precipitation Climatology Project (GPCP; Adler et al. 2003) and Tropical Rainfall Measuring Mission (TRMM) 3B42. Convective and stratiform rain products from TRMM are used in the study. Monthly products such as wind patterns, precipitable water, and temperature from NCEP reanalysis version 2 (Kanamitsu et al. 2002) are also utilized in the analysis. The Modern-Era Retrospective Analysis for Research and Application Analysis (MERRA) monthly product between 2001 and 2011 has been used for cloud ice and cloud water hydrometeors. Detailed description of MERRA v5.2.0 dataset is available in recent work of Rienecker et al. (2011). The cloud fraction dataset from the Cloud-Aerosol Lidar with Orthogonal Polarization (CALIOP) instrument on board the Cloud-Aerosol Lidar and Infrared Pathfinder Satellite Observations (CALIPSO) satellite is used here (Hu et al. 2009; Winker et al. 2009; Thorsen et al. 2011; Hazra et al. 2015a). The monthly June–September (JJAS) climatology product of cloud fraction from 2006–2012 have been used for the calculation of high cloud fractions. NOAA interpolated outgoing longwave radiation (OLR; Liebmann and Smith 1996) is also used in the present study.

## 3 Results and discussions

### 3.1 Performance of microphysical schemes in terms of rainfall

The simulation of the rainfall patterns by dynamical model over Indian region has been proved to be a difficult task due to its extremely complex spatial distribution and large precipitation gradients. This may pose difficulty in replicating the exact pattern with the correct amplitude (Kulkarni et al. 2010). However, a model which is able to simulate the observed climatological mean more closely also have a propensity to



have a better prediction skill (e.g., Delsole and Shukla 2010). Therefore, climatological mean features have utmost importance for understanding the improvements in the skill of model. The major observed features of ISMR captured well by the CFSv2 experiments (i.e., ZC90, BF90, ZC95, BF95) are primary continental rain belt extending from the Bay of Bengal across the Indo-Gangetic plains corresponding to the monsoon trough and the low pressure systems, secondary oceanic rain belt near the equatorial regions around 5° S (Fig. 1a–e). Other features include rainfall maximum over west coast due to the Western Ghats orographic barrier, maximum rainfall over northeast India associated with the Himalayan orography, and low rainfall over the southeast peninsula (Fig. 1a–e). Region of mini-cold pool region off the southern tip of India (e.g., Joseph et al. 2005; Rao et al. 2006) marked by very low rainfall is also well simulated by the CFSv2 experiments (Fig. 1a–e).

CFSv2 simulations depict dry rainfall bias over central Indian region (CFSv2 rainfall bias: Fig. 2a–d). However,

relatively less dry bias is noted in ZC90 (Fig. 2a) with respect to observed rainfall (GPCP). ZC90 and ZC95 show pattern correlation of 0.7 with respect to observation (GPCP). In case of BF90, pattern correlation come out to be 0.6, and for BF95, it is very low as 0.3. ZC90-simulated rainfall patterns are relatively better over central India as compared to BF90 (Fig. 2e, see also Table 1). BF90, BF95, and ZC95 experiments are not able to show any improvement over central Indian region (Fig. 2f–h). In case of ZC90, BF90, and ZC95 experiments, equatorial Indian Ocean region exhibits wet bias over entire basin except some part of central equatorial Indian Ocean region (Fig. 2a–c). However, in case of BF95, entire Indian Ocean basin has prevalent wet bias (Fig. 2d). Northeast Indian region and eastern equatorial Indian region is dominated by wet bias in BF95 experiment, which is quite unrealistic (Fig. 2d). Ferrier et al. (2002) scheme (hereafter BF) with high RHcrit (i.e., 95 %) seems to produce more rainfall over heavy rainfall regions of Indian landmass and also over oceanic regions.

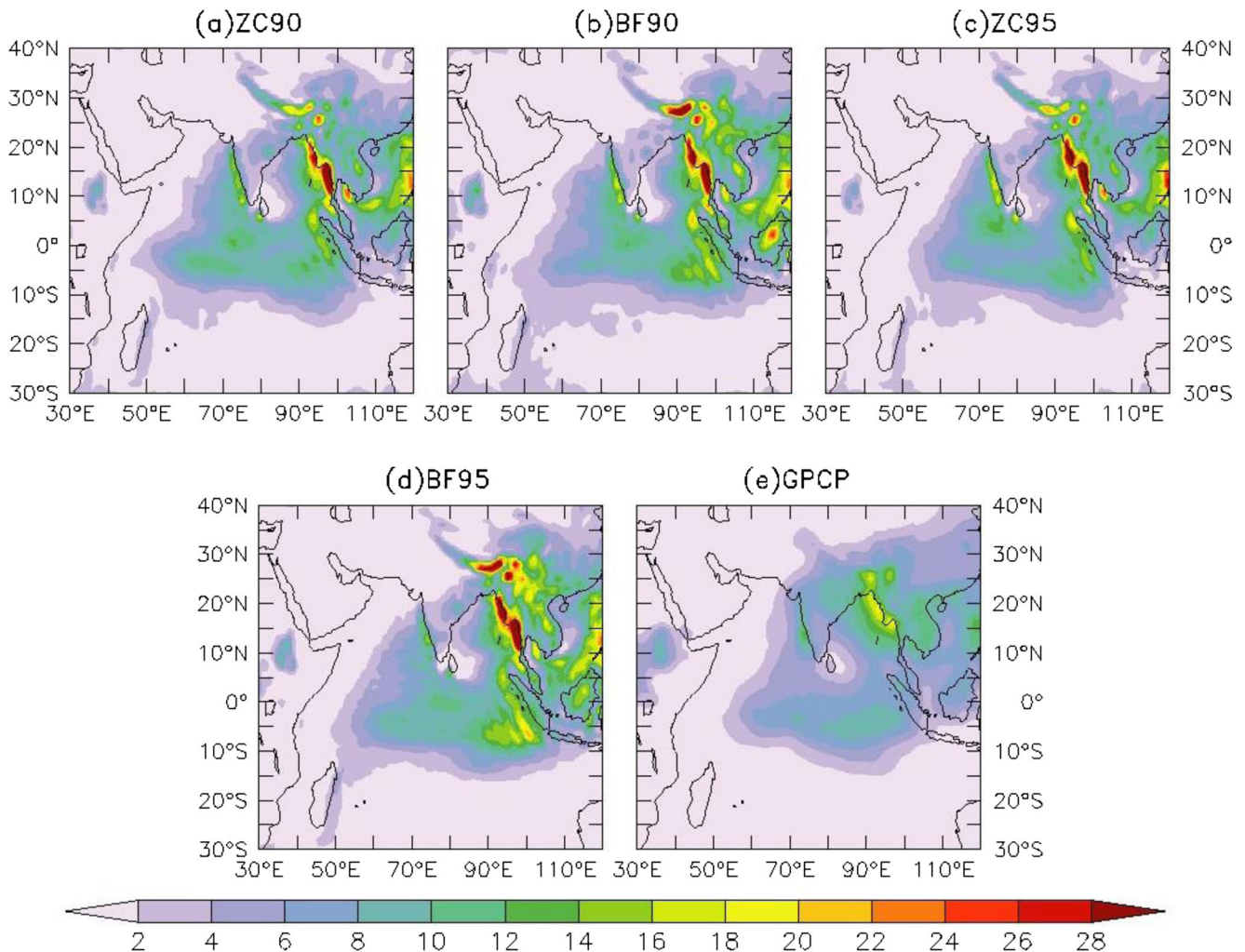


**Fig. 1** CFSv2-simulated JJAS (June–September) rainfall (mm/day) climatology for **a** ZC90, **b** BF90, **c** ZC95, and **d** BF95. Corresponding GPCP-based JJAS rainfall climatology is also presented (**e**)

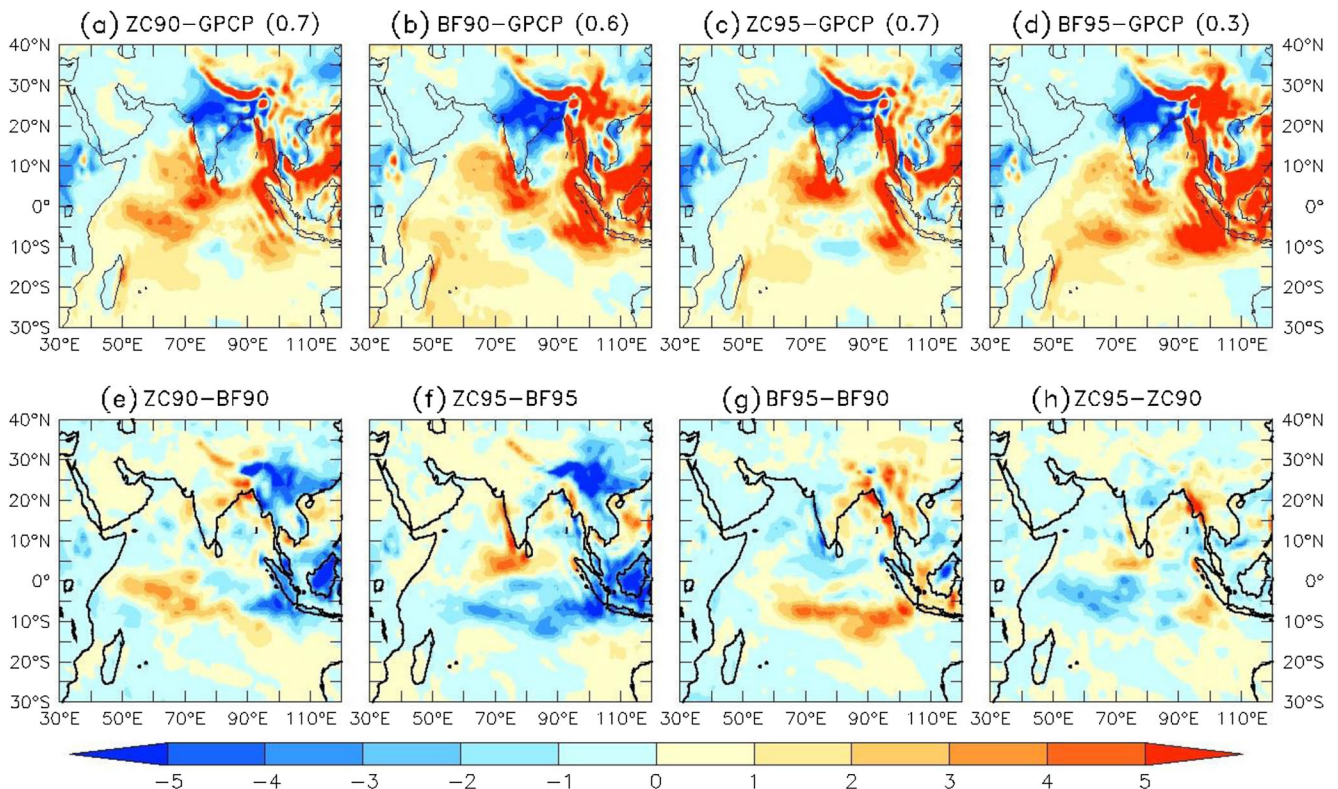


**Fig. 2** Model rainfall bias (i.e., difference between JJAS rainfall climatology of CFSv2 and GPCP, unit: mm/day) for **a** ZC90 (i.e., ZC90-GPCP), **b** BF90 (i.e., BF90-GPCP), **c** ZC95 (i.e., Z95-GPCP), **d**

BF95 (i.e., BF95-GPCP). Difference between the individual experiments is presented as **e** ZC90-BF90, **f** ZC95-BF95, **g** BF95-BF90, and **h** ZC95-ZC90

JJAS mean and standard deviation for ISMR (averaged over larger domain of Indian region: 5° N–35° N, 65° E–95° E) are presented in Table 2. It was computed based on 9 years of JJAS mean (since first year is excluded for the model spinup). ZC-simulated JJAS mean is relatively better than that of BF simulated (see Table 2). In terms of standard deviation (SD), ZC95 and BF95 show better performance which is comparable with observation. However, in terms of both JJAS mean and SD, ZC95 is relatively better. BF90-simulated JJAS mean is relatively low (i.e., 5.3), and it has very large SD (0.9). BF95-simulated JJAS mean is largely underestimated (i.e., 5.2). Overall ZC has simulated better mean and interannual variability as compared to BF.

Model-simulated ZC and BF experiments are able to depict the observed SD of JJAS rainfall (Fig. 3a–e). High raining regions such as Western Ghats, northeast regions of India, and tropical Indian Ocean regions are marked by high standard deviation of JJAS rainfall (see observation; Fig. 3e). ZC and BF are able to capture these characteristics features reasonably well (Fig. 3a–d). However, slight overestimation of SD is noted in case of ZC90, BF90, and BF95. ZC95-simulated SD is relatively in good agreement with observation. As a result, interannual variability exhibited by ZC95 is relatively better as compared to others.

**Table 1** JJAS rainfall bias (model—GPCP) over Indian region (averaged over 70° E–90° E, 10° N–25° N; unit: mm/day) for ZC90, BF90, ZC95, and BF95

	ZC90	BF90	ZC95	BF95
Rainfall bias over Indian region (averaged over 70° E–90° E, 10° N–25° N; unit: mm/day)	-3.5	-4.4	-4.0	-3.9

**Table 2** JJAS mean and standard deviation for ISMR (averaged over 5° N–35° N, 65° E–95° E) for ZC90, BF90, ZC95 experiments and for observation based on TRMM 3B42

Experiment name	JJAS mean (mm/day)	Standard deviation (SD; mm/day)
ZC90	5.4	0.7
BF90	5.3	0.9
ZC95	5.4	0.5
BF95	5.2	0.5
TRMM 3B42 (observation)	5.7	0.4



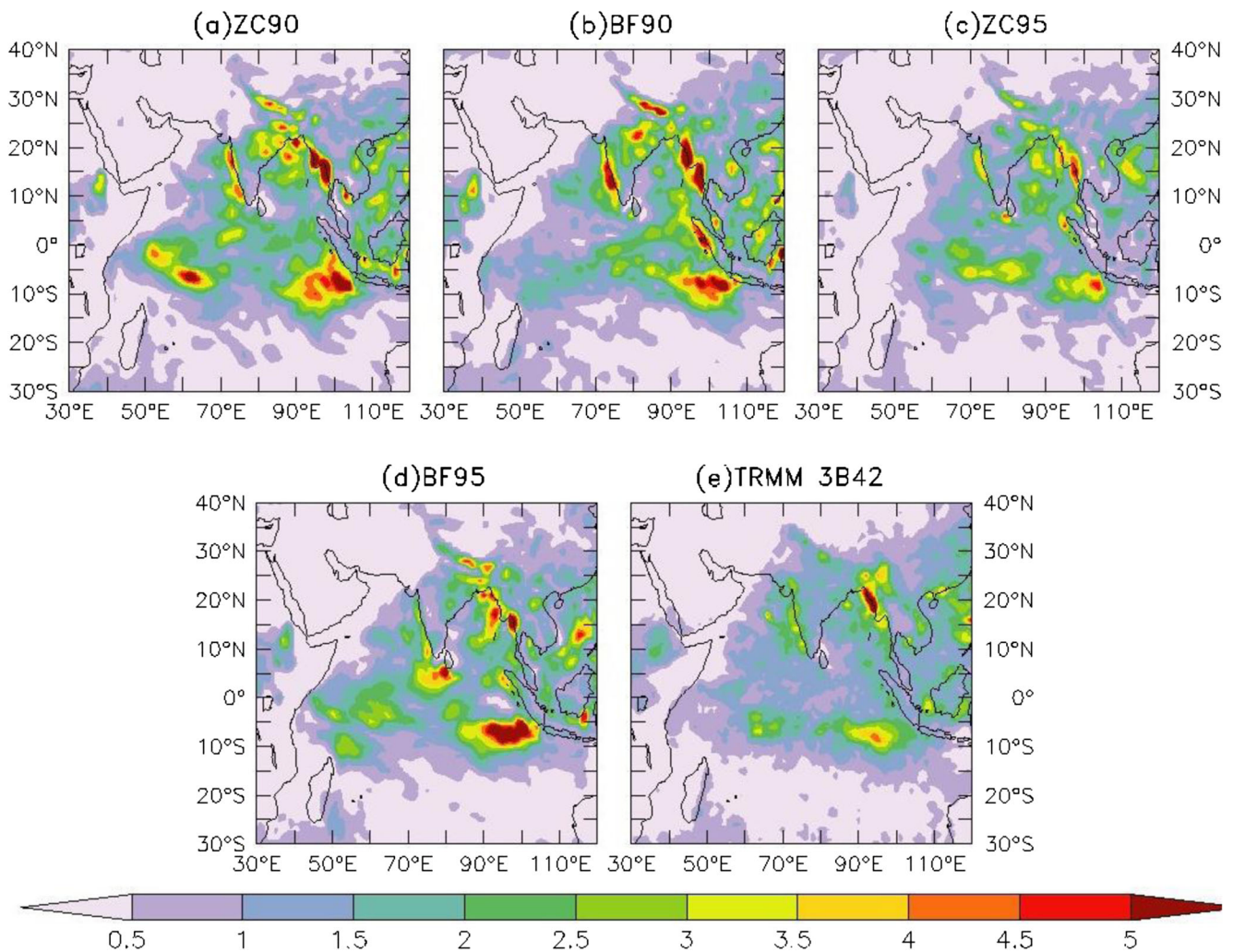


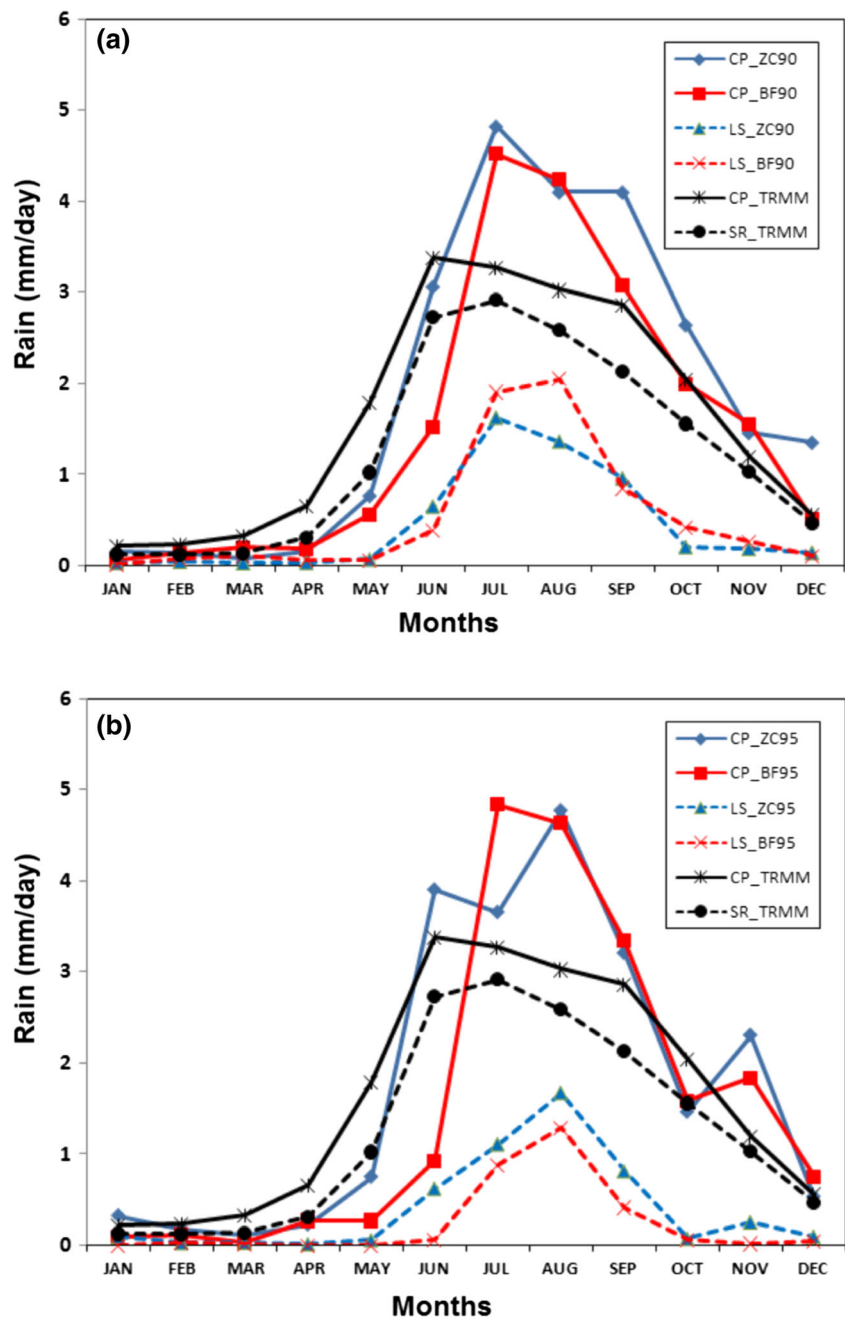
**Fig. 3** Standard deviation (unit: mm/day) of JJAS rainfall for **a** ZC90, **b** BF90, **c** ZC95, **d** BF95 (based on 9 years of CFSv2 simulations), and for **e** observation (based on TRMM 3B42 dataset for the period 1998–2009)

Further, we have examined convective and large-scale rain from the simulation of different microphysical schemes (ZC and BF; Fig. 4a–b). It reveals that both the schemes overestimate (underestimate) the convective rain (large-scale rain/stratiform rain). Annual cycle pattern of convective rain of ZC90 resembles (differs) with observation during onset (withdrawal) phase of ISM (Fig. 4a). The annual cycle of convective rain for ZC95, in case of onset and withdrawal of ISM, is comparable with observation (Fig. 4b). However, JJAS mean of ZC95 depicts variations, and it overestimates as compared to observation. In contrast, the annual cycle of BF90 and BF95 depict reasonable patterns during withdrawal as compared to onset of ISM. For large-scale rain, both microphysical schemes (ZC and BF) portray similar patterns during onset and withdrawal of ISM. However, ZC90 produces relatively less large-scale rain as compared to BF90. In contrast, there is less difference in large-scale rain of ZC95 and BF95. As a result, annual cycle (for ZC95 and BF95) patterns are also similar.

### 3.2 Precipitable water

Precipitable water (PW) is an important variable of the model as it is manifested in surface precipitation. In general, PW mimics the rainfall patterns in observations (Fig. 5e). CFSv2-simulated PW for ZC90, BF90 and ZC95 experiments also resemble with corresponding rainfall patterns (Fig. 5a–c). However, BF95 shows overestimation of PW over northeast Indian land mass region and over most of the oceanic warm pool region (mean: Fig. 5d, bias: Fig. 6d). This land and marine-based atmospheric moisture may contribute in excess rainfall activity by precipitating out (e.g., Trenberth and Guillemot 1998; Misra et al. 2012) over these regions. As a result, BF95 shows excess rainfall in Indian Ocean basin region (wet bias seen in Fig. 2d). CFSv2 exhibits negative PW bias over northern and central Indian region in all experiments (Fig. 6a–d), which is also in line with rainfall bias (Fig. 2a–d). However, ZC90-simulated pattern demonstrates improvement in this northern and central Indian region PW bias as

**Fig. 4** Annual cycle of convective (CP)/large-scale (LS) rain from two microphysical schemes (i.e., ZC and BF) for **a** 90 % RHcrit and **b** 95 % RHcrit. For observational purpose, TRMM convective (CP\_TRMM) and stratiform (SR\_TRMM) rain are used



compared to other experiments (Fig. 6e–h). BF scheme shows larger variation in PW patterns, which is clear from Fig. 6g (induces heavy PW in case of BF95) as compared to ZC scheme (where moderate changes are taking place; Fig. 6h). Overall, ZC90 scheme performance seems to be optimal.

### 3.3 Lower and upper tropospheric circulation

The dominant features of the monsoon circulation over south Asian region are the cross-equatorial flow (Findlater jet) from

Southern Hemisphere along the east coast of Africa, southwesterly/westerly flow over the Arabian Sea, Indian peninsula and Bay of Bengal (Fig. 7e; observed winds at 850 hPa). Findlater jet transports moisture from the southern Indian Ocean to Indian landmass by connecting the Mascarene High and Indian monsoon trough and forms the lower branch of Hadley cell. CFSv2-simulated wind patterns (ZC90, BF90, ZC95, and BF95) are also able to depict the conspicuous feature of Findlater jet (Fig. 7a–d). Among model simulation, differences are minimal (see Table 3, Findlater jet core speed averaged over 46° E–65° E, 5° N–15° N).

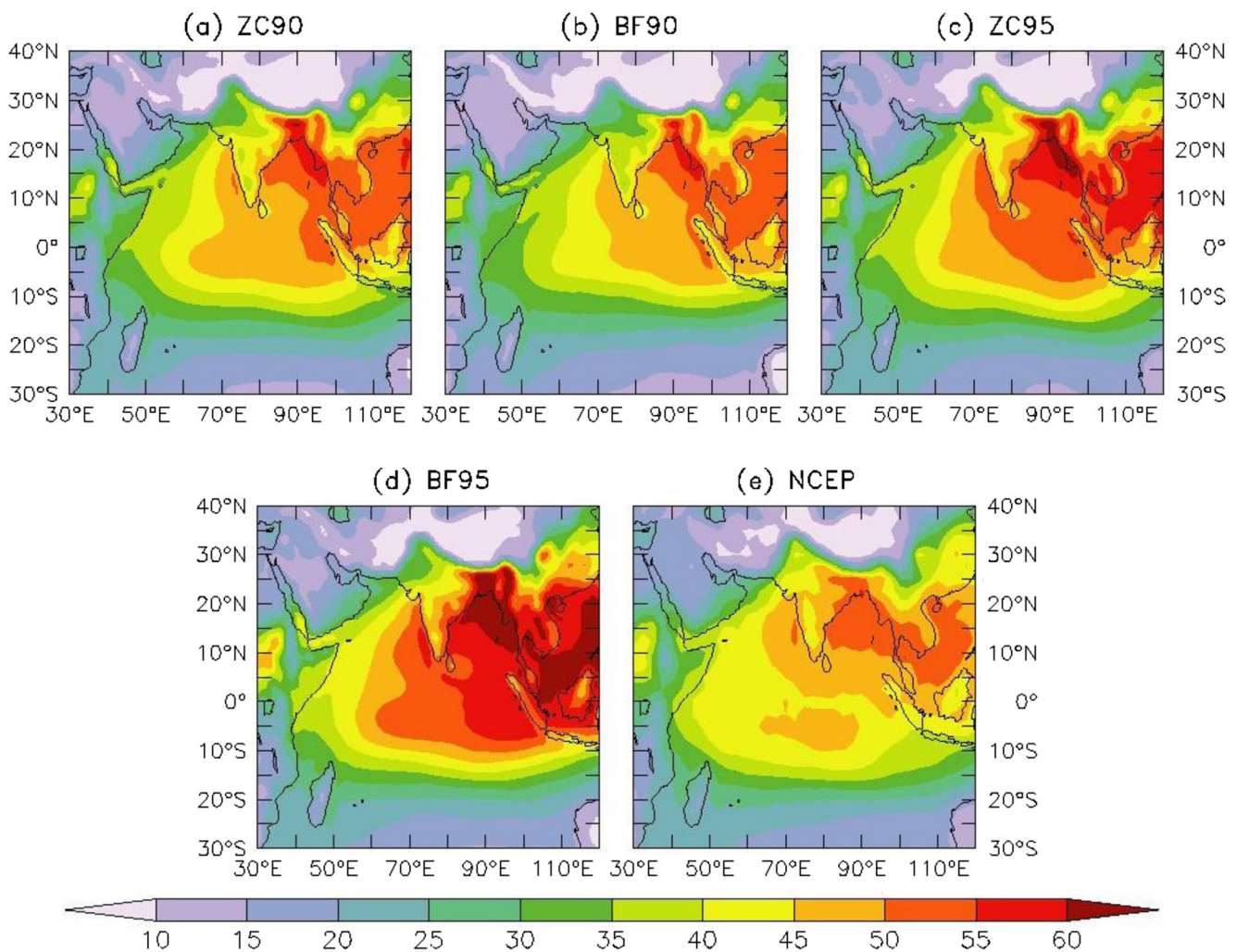


**Fig. 5** CFSv2-simulated JJAS precipitable water climatology (%) for **a** ZC90, **b** BF90, **c** ZC95, and **d** BF95. Corresponding NCEP-based JJAS precipitable climatology is also presented (**e**)

Sometimes, a dynamic instability of the Findlater jet can occur leading to a real split of the jet near Somalia creating two jets over India–Sri Lanka longitudes (Thompson et al. 2008). This splitting of jet could be a temporary feature associated with break spell (Joseph and Sijikumar 2004), and it could be a feature of the transition between a dry and a wet spell of the monsoon (Thompson et al. 2008). However, dominance of northern jet (southern jet) might play an important role for the strengthening (weakening) of monsoon (e.g., Thompson et al. 2008). When the northern jet alone is dominant, the Indian monsoon tends to be wetter. When the southern jet alone is dominant, the monsoon is drier (Thompson et al. 2008). In case of ZC simulations, northern jet is dominant. As a result, ZC-simulated monsoon can be wetter, which may lead to better JJAS mean. In case of BF simulations, southern jet is dominant which may lead to relatively drier monsoon.

In the upper troposphere (at 200 hPa), CFSv2 experiments (ZC90, BF90, ZC95, and BF95) are able to depict a prominent

observed circulation system of Asian monsoon in terms of Tibetan High (Fig. 8a–e). Tibetan anticyclone contains an easterly jet stream in its southern flank called as tropical easterly jet (TEJ). TEJ is located over the southern India and adjoining equatorial Indian Ocean. This characteristic feature of TEJ is well captured by the CFSv2 experiments, although its strength is underestimated (Fig. 8a–e; Table 3). Strength of TEJ is related with the monsoon activity over the Indian subcontinent (Naidu et al. 2011; Chaudhari et al. 2013). ZC90-simulated TEJ strength is 15.4 m/s which is underestimated as compared to observation (which has TEJ strength as 19.2 m/s). However, it is relatively better than that of ZC95 (15.0 m/s). Although BF-simulated TEJ strength is more close to observations, it is contaminated by more dry bias over Indian region.

Overall, CFSv2 is able to depict these features; however, simulated wind patterns are underestimated in upper troposphere. Microphysical schemes might be responsible for this moderate success of depicting upper tropospheric circulation which will be discussed in the next section.



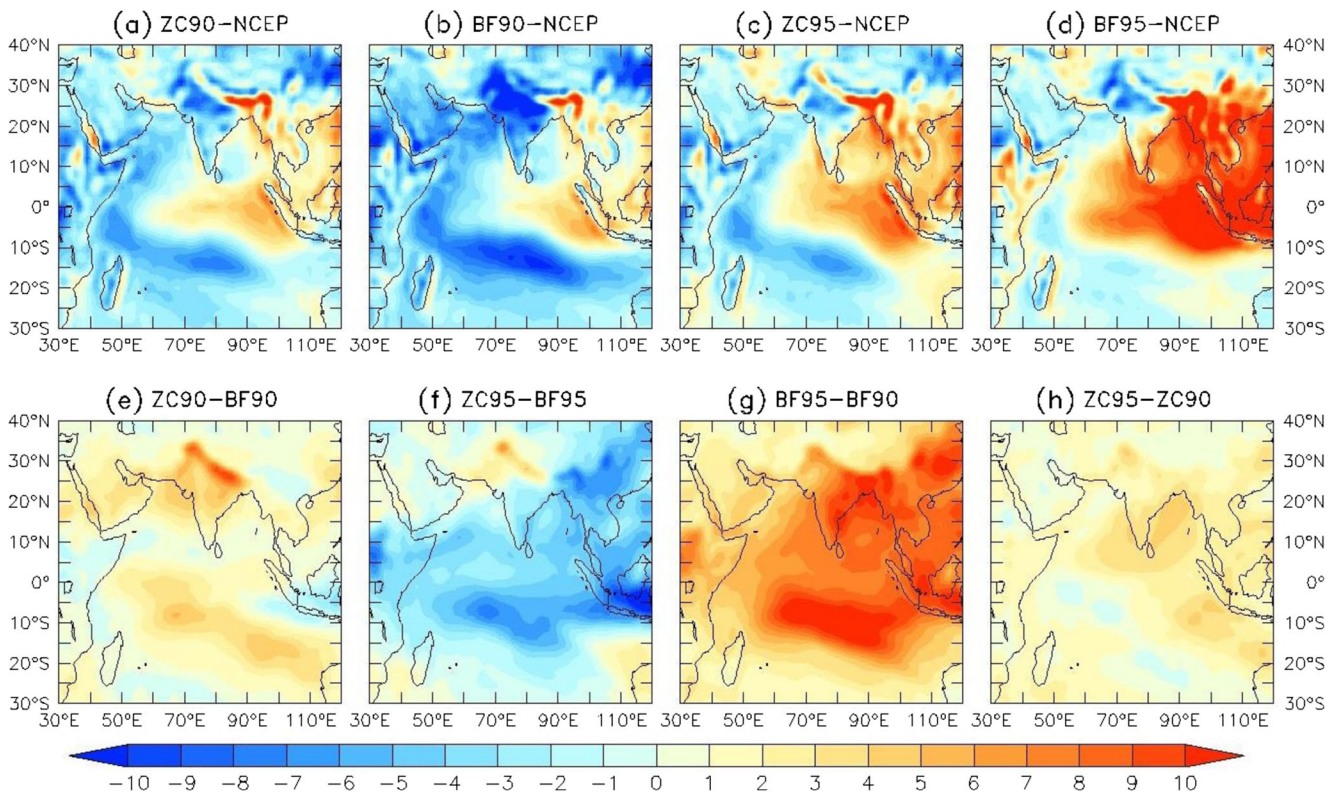


**Fig. 6** Model precipitable water bias (i.e., difference between JJAS precipitable water climatology of CFSv2 and GPCP, unit: mm/day) for **a** ZC90 (i.e., ZC90-GPCP), **b** BF90 (i.e., BF90-GPCP), **c** ZC95 (i.e.,

Z95-GPCP), **d** BF95 (i.e., BF95-GPCP). Difference between the individual experiments is presented as **e** ZC90-BF90, **f** ZC95-BF95, **g** BF95-BF90, and **h** ZC95-ZC90

### 3.4 Total cloud condensate, high-level cloud fractions, and outgoing longwave radiation

Spatial pattern of total cloud condensate is relatively better represented by ZC schemes as compared to BF schemes (Fig. 9a–e), although it is underestimated over Indian landmass region as compared to MERRA. Regarding BF, simulated total cloud condensate patterns are better over Indian landmass. However, it is highly overestimated over northeast region, which is unrealistic. To get the further details, vertical profile of total cloud condensate is presented (Fig. 10). Vertical profile is not properly represented in BF schemes, and it has huge overestimation (underestimation) over lower (upper) level (Fig. 10). In this context, ZC-simulated total cloud condensate profile is better at upper and lower level (Fig. 10) as compared to BF. Upper level cloud condensate may have effect on high cloud fractions and tropospheric temperature. To investigate it further, high cloud fraction is presented in Fig. 11 along with corresponding satellite observation of CALIPSO. Relatively more total cloud condensate at upper level is reflected in more high cloud fraction in ZC as compared to BF (see Fig. 11a–e). Although high cloud fraction is underestimated over Indian region, it is relatively

close to observations in ZC as compared to BF (Fig. 11a–e). In brief, ZC-simulated high cloud fraction (Fig. 11a, c) is in relatively good agreement with observation (CALIPSO; Fig. 11e).

As discussed earlier, total cloud condensate will also modulate tropospheric temperature (TT) and tropospheric temperature gradient which play major role in monsoon circulation. ZC90 and ZC95 depict cold bias in TT (Fig. 12a, c). It is in line with previous studies of Saha et al. (2014b). BF90 has strong cold bias (Fig. 12b). In contrast, BF95 has warm TT bias (Fig. 12d), which is unrealistic. Overall, ZC90 has somewhat reduced cold TT bias as compared to BF90, which could be beneficial for the monsoon circulation.

Previous studies have demonstrated that OLR is a reasonable indicator of the convective activity over the tropical regions which are strongly influenced by cloudiness, and it varies directly with cloud top temperature (Krishnamurti et al. 1989). The region of low OLR indicates the region of intense convection which is associated with monsoon (e.g., Kripalani et al. 1991; Chaudhari et al. 2010). Observation depicts dominance of low OLR (represented in blue color) in monsoon zone (Fig. 13e). In case of BF, OLR values are

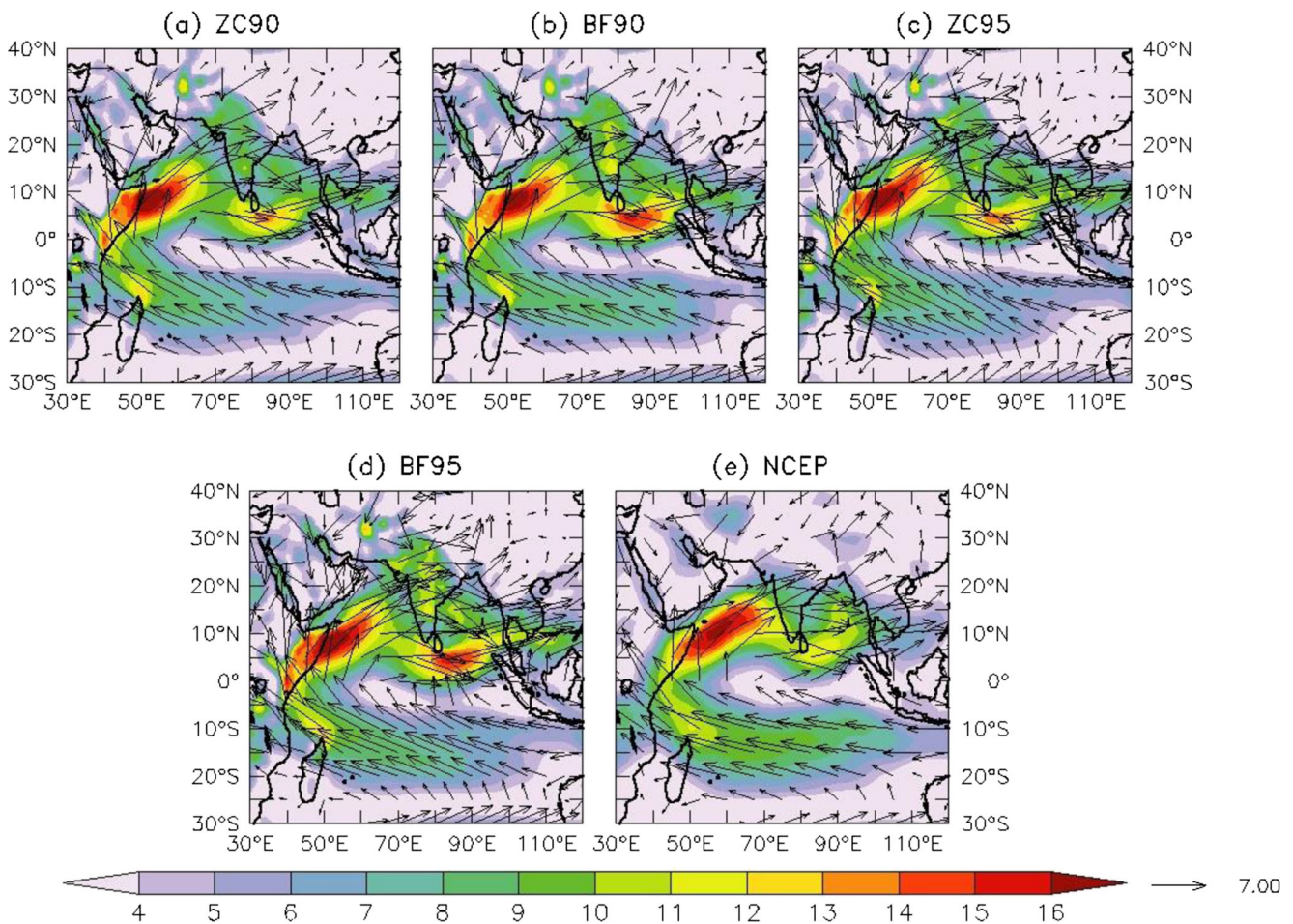


**Fig. 7** CFSv2-simulated climatological JJAS wind patterns at 850 hPa (unit: m/s) for **a** ZC90, **b** BF90, **c** ZC95, and **d** BF95. Corresponding NCEP-based JJAS wind patterns at 850 hPa is also presented (**e**)

relatively high (Fig. 13b, d) indicating weaker and shallow convection. ZC-simulated OLR is in good agreement with observation as compared to BF (Fig. 13a–e). As a result, ZC-simulated rainfall pattern will be better than that of BF. Hazra et al. (2015a) have demonstrated that high-level cloud fraction and convective activity in terms of OLR is highly correlated. As we have seen that ZC has relatively better high cloud fraction as compared to BF (Fig. 11a–e), it is reflected well in OLR patterns of ZC (Fig. 13). Possible reasons for the same are explored in the following section.

### 3.5 Possible reasons and physical processes responsible for exploring the link between clouds and ISMR

The interaction among thermodynamics, cloud microphysics, and dynamics plays a vital role in the summer monsoon precipitating clouds (Hazra et al. 2013a, b; Kumar et al. 2014). In case of BF, relatively high OLR (Fig. 13b, d) as compared to observation is seen in monsoon zone which indicates weaker convection having weaker updrafts. As a result, lesser upper level cloud condensate (Fig. 10) is noted in BF. We have seen that vertical profile of cloud (Fig. 10) is

**Table 3** JJAS Findlater jet core wind speed (averaged over 46° E–65° E, 5° N–15° N; unit: m/s; at 850 hPa) for ZC90, BF90, ZC95, BF95, and NCEP

	ZC90	BF90	ZC95	BF95	NCEP
Findlater jet core wind speed (averaged 46° E–65° E, 5° N–15° N; unit: m/s)	12.5	12.2	12.6	12.5	12.4
TEJ (averaged 70° E–90° E, 10° N–15° N; unit: m/s)	15.4	18.3	15.0	16.8	19.2

Similarly, JJAS tropical easterly jet (TEJ, averaged over 70° E–90° E, 10° N–15° N; unit: m/s; at 200 hPa) is also presented for ZC90, BF90, ZC95, BF95, and NCEP



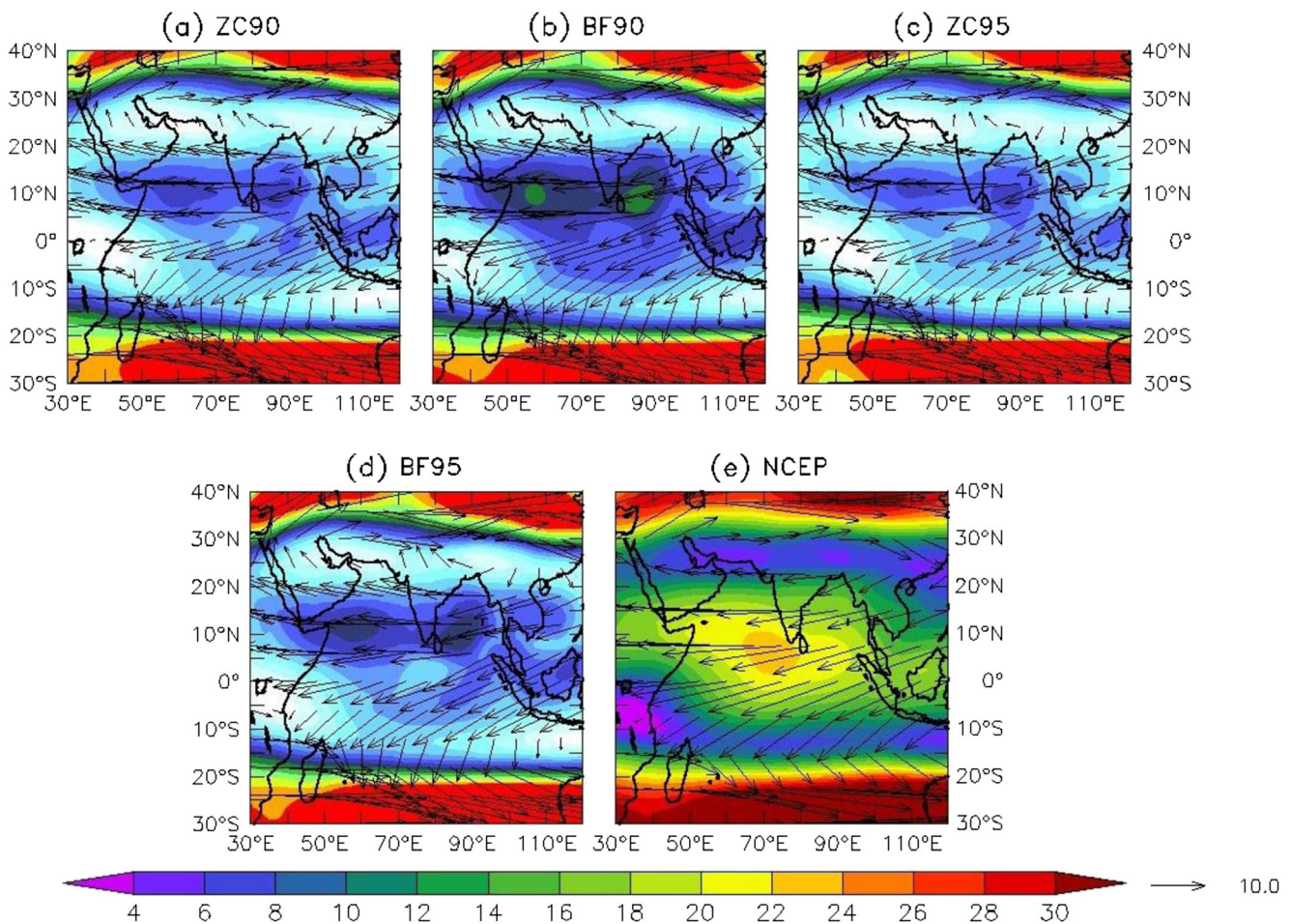


**Fig. 8** CFSv2-simulated climatological JJAS wind patterns at 200 hPa (unit: m/s) for **a** ZC90, **b** BF90, **c** ZC95, and **d** BF95. Corresponding NCEP-based JJAS wind patterns at 200 hPa is also presented (**e**)

not properly represented in BF schemes, and it illustrates overestimation (underestimation) at lower (upper) level. This less cloud condensate at upper level of BF (due to less deposition and condensation processes) will produce weaker latent heating, and more cloud condensate at lower level will result in cooling through cloud water evaporation (e.g., Kumar et al. 2014; Hazra et al. 2013a, b; Tao et al. 1990). This improper vertical structure of heating/cooling results in suppressed convection during ISM (as revealed by relatively high OLR in BF; Fig. 13b, d). Less cloud condensate at upper level will lead to low high-level cloud fraction in BF schemes. It will provide feedback to OLR making it relatively high. These interactions/processes can be broadly summarized by a feedback loop as shown by the schematic diagram (Fig. 14b).

ZC simulations depict relatively better OLR (Fig. 13a, c) in monsoon region (relatively closer to observation; Fig. 13e) which indicates strong convection having strong updrafts. Consequently, more upper level cloud condensate (Fig. 10) is shown in ZC. Vertical profile of cloud condensate

(Fig. 10) is also relatively better in ZC schemes, and it is close to MERRA as compared to BF. This more cloud condensate at upper level of ZC (due to better portrayal of freezing, deposition, and condensation processes) will produce stronger latent heating and will lead to relatively strong convection during ISM as exhibited by relatively low OLR. More cloud condensate at upper level may lead to more high-level cloud fraction in ZC schemes. It may provide feedback to OLR making them relatively low. It is also illustrated by a feedback loop as shown by the schematic diagram (Fig. 14a).

#### 4 Conclusions

Impact of microphysical schemes of CFSv2 on Indian summer monsoon is investigated in the present study. Previous studies (e.g., Sanderson et al. 2010) have highlighted the benefit of a proper prescription of RHcrit for better portrayal of cloud processes and consequently the betterment of ISM simulations in coupled ocean atmosphere simulations. Thus, sensitivity experiments with different RHcrit (90 and 95 %) are



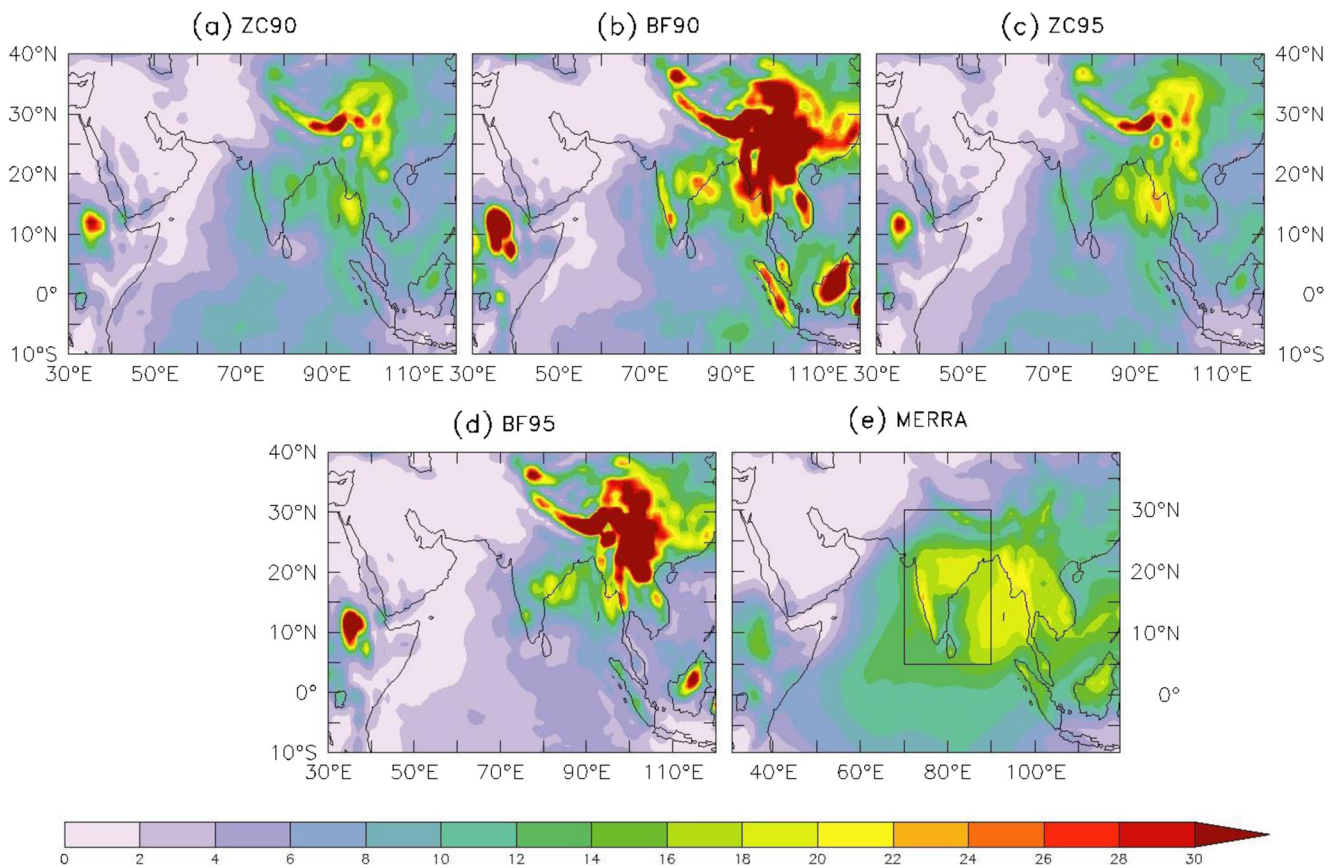


**Fig. 9** CFSv2-simulated climatological JJAS total cloud condensate (mg/kg) for **a** ZC90, **b** BF90, **c** ZC95, and **d** BF95. Corresponding MERRA-based climatology of total cloud condensate is also presented (**e**)

performed along with different microphysical schemes (ZC and BF). The salient features of the study are elaborated pointwise:

1. Climatological mean features in terms of rainfall are better represented by all the sensitivity experiments. ZC90 and ZC95 exhibit better map-to-map correlation (i.e., 0.7) as compared to BF schemes (which varies from 0.6–0.3). Dry bias over Indian region is also reduced in case of ZC90. BF95 depicts more rainfall over heavy rainfall regions of Indian landmass and over oceanic regions. Performance of ZC90 is relatively better in terms of rainfall. However, both microphysical schemes (i.e., ZC and BF) reveal that both the schemes overestimate (underestimate) the convective rain (large-scale rain).
2. Precipitable water (PW) simulations from ZC90, BF90, and ZC95 mimic corresponding rainfall patterns. However, BF95 shows overestimation of PW over north-east Indian land mass region and over larger part of the oceanic warm pool region. Therefore, BF95 shows excess rainfall in Indian Ocean basin region, which seems to be unrealistic.
3. Lower tropospheric circulation of model is well depicted by all the experiments. Model is able to depict the

- characteristic feature of Findlater jet. In ZC simulations, northern jet is dominant. As a result, ZC-simulated monsoon can be wetter, which may lead to better JJAS mean (which is relatively close to observation). In case of BF simulations, southern jet is dominant which may lead to relatively drier monsoon (e.g., Thompson et al. 2008). In the upper troposphere (at 200 hPa), all CFSv2 experiments are able to depict a conspicuous feature of circulation system of Asian monsoon in terms of Tibetan High. TEJ is also well replicated by all the experiments; however, its strength is underestimated in all the experiments. In nutshell, CFSv2 is able to depict these features; however, simulated wind patterns are underestimated in upper troposphere. This underestimation could be linked with improper representation of cloud condensate at upper level.
4. Spatial pattern of total cloud condensate is relatively better recapitulated by ZC schemes as compared to BF schemes. Vertical profile of total cloud condensate is not properly simulated in BF schemes, which is overestimated (underestimated) at lower (upper) level. ZC-simulated total cloud condensate profile is relatively close to observation, and it is better at upper and lower

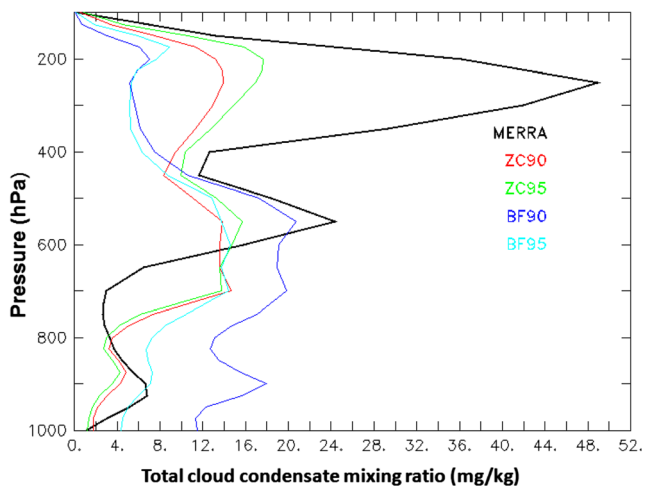


**Fig. 10** Vertical profile of JJAS total cloud condensate mixing ratio (mg/kg) averaged over 70° E–90° E, 5° N–30° N for MERRA (black line), ZC90 (red line), ZC95 (green line), BF90 (navy blue line), and BF95 (aqua line)

level. Relatively more total cloud condensate at upper level has lead to relatively better high cloud fraction in ZC simulation.

- Physical processes which accentuate the linkage between clouds and ISMR can be explained by a feedback represented by schematic diagram (Fig. 14a–b). Relatively

high OLR, which is an indicative of weaker convection having weaker updrafts, is noted in BF simulation over monsoon zone. Subsequently, less upper level cloud condensate is seen in BF. It can be due to improper representation vertical profile of cloud, which shows underestimation (overestimation) of upper (lower) level cloud condensate. This less cloud condensate at upper level of BF may generate weaker latent heating, and more cloud condensate at lower level may result in cooling through cloud water evaporation. Thus, this improper vertical structure of heating/cooling results in suppressed convection during ISM season as exhibited by relatively high OLR in BF. Less cloud condensate at upper level will lead to low high-level cloud fraction in BF schemes which will provide feedback to OLR making them relatively high.

- ZC simulations represent low OLR, which has great proximity with observation. It implies strong convection having stronger updrafts. Accordingly, more upper level cloud condensate is exhibited in ZC. Vertical profile of cloud is also relatively better represented by ZC schemes. This more cloud condensate at upper level of ZC (which is in agreement with observation) will produce stronger latent heating and will lead to relatively strong convection during ISM as marked by relatively low OLR. More cloud condensate at upper level will correspond to more

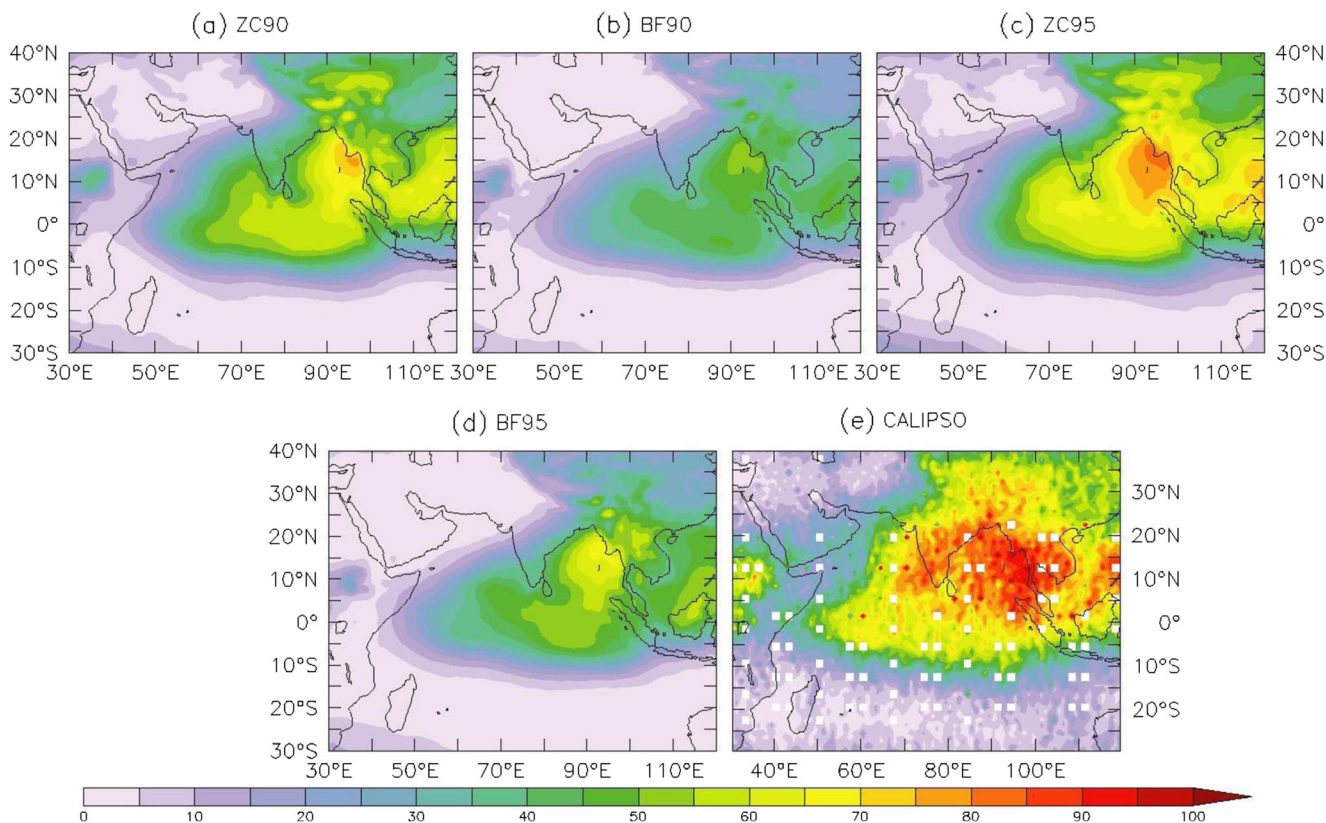


**Fig. 11** CFSv2-simulated climatological JJAS high cloud fractions for a ZC90, b BF90, c ZC95, and d BF95. Corresponding CALIPSO-based JJAS high cloud fractions are also presented (e)



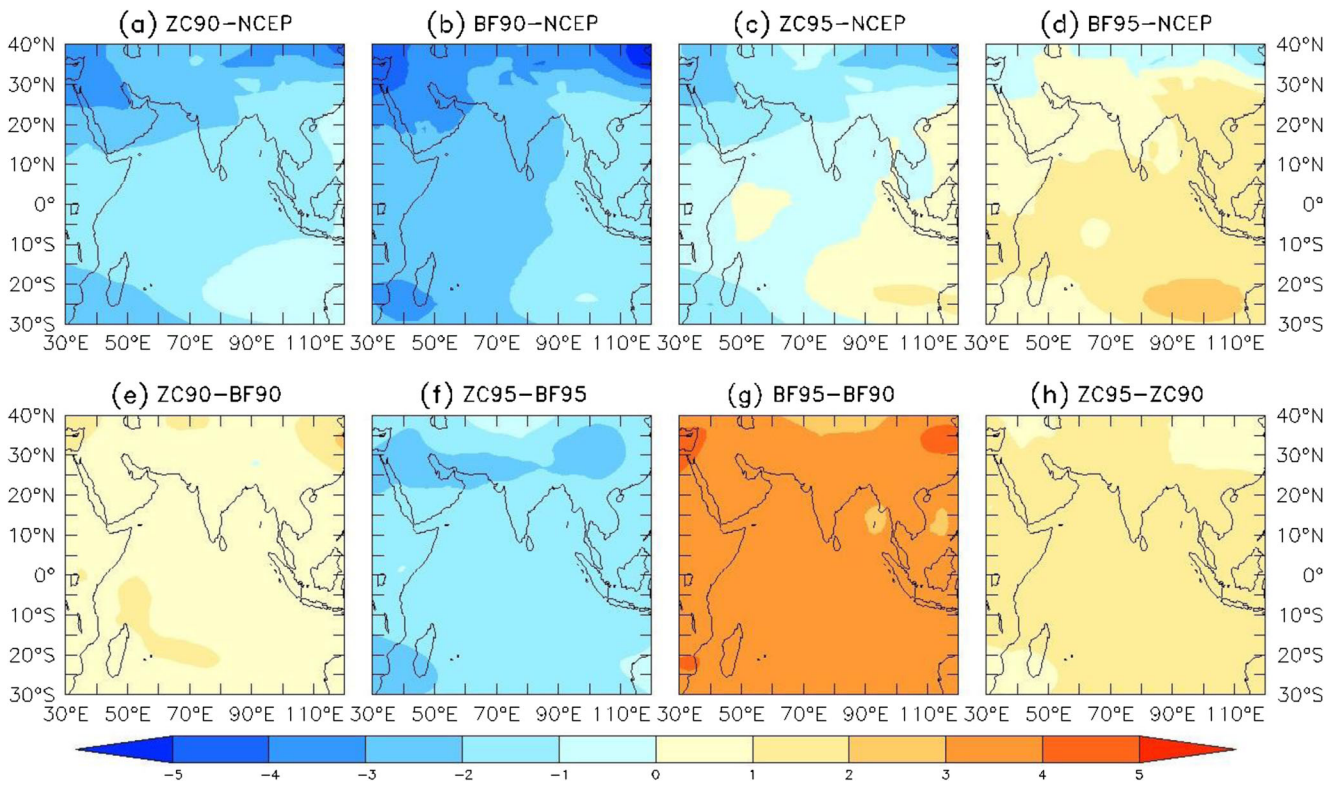


**Fig. 12** Model-simulated tropospheric temperature (TT) bias (i.e., difference between JJAS TT of CFSv2 and NCEP, unit: °C) for **a** ZC90 (i.e., ZC90-GPCP), **b** BF90 (i.e., BF90-GPCP), **c** ZC95 (i.e., Z95-GPCP), and **d** BF95 (i.e., BF95-GPCP). Difference between the individual experiments is presented as **e** ZC90-BF90, **f** ZC95-BF95, **g** BF95-BF90 and **h** ZC95-ZC90

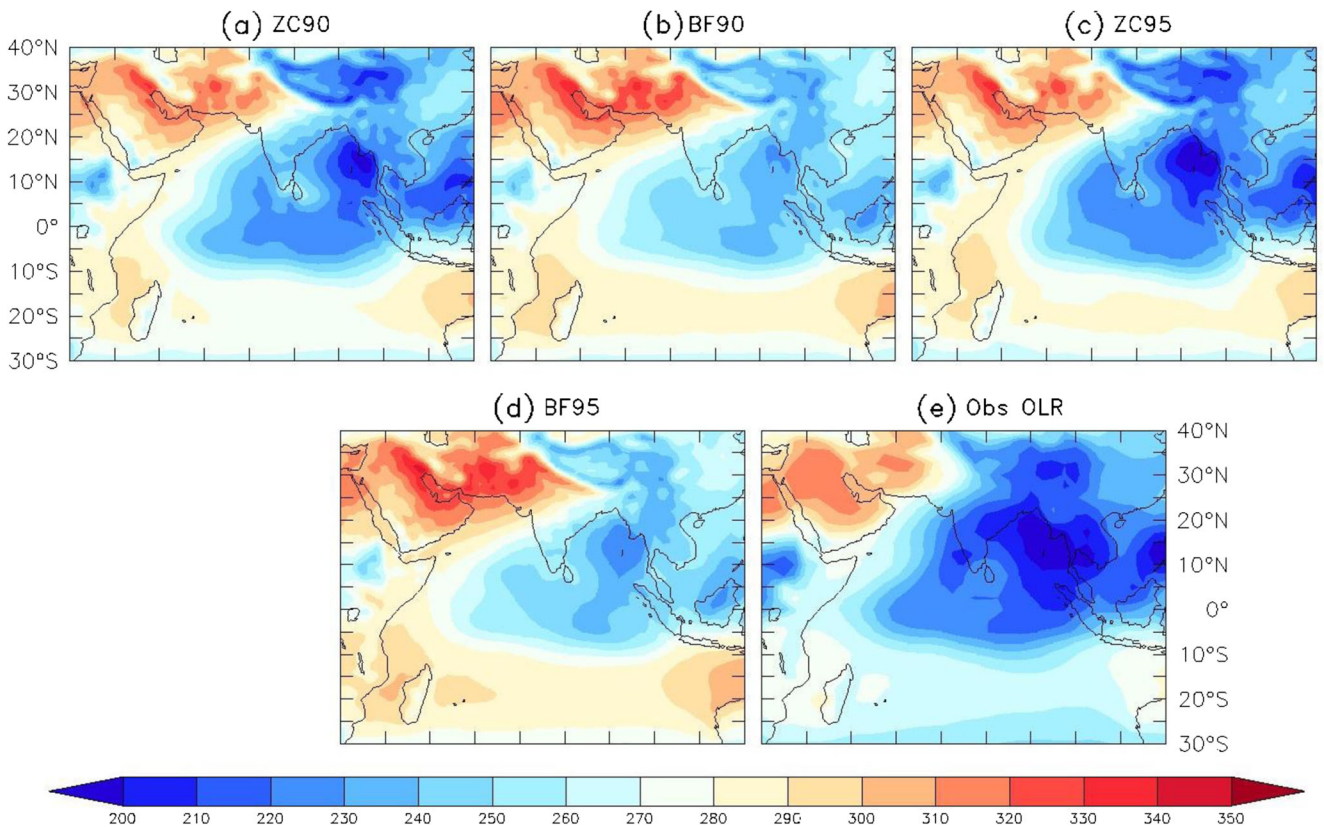
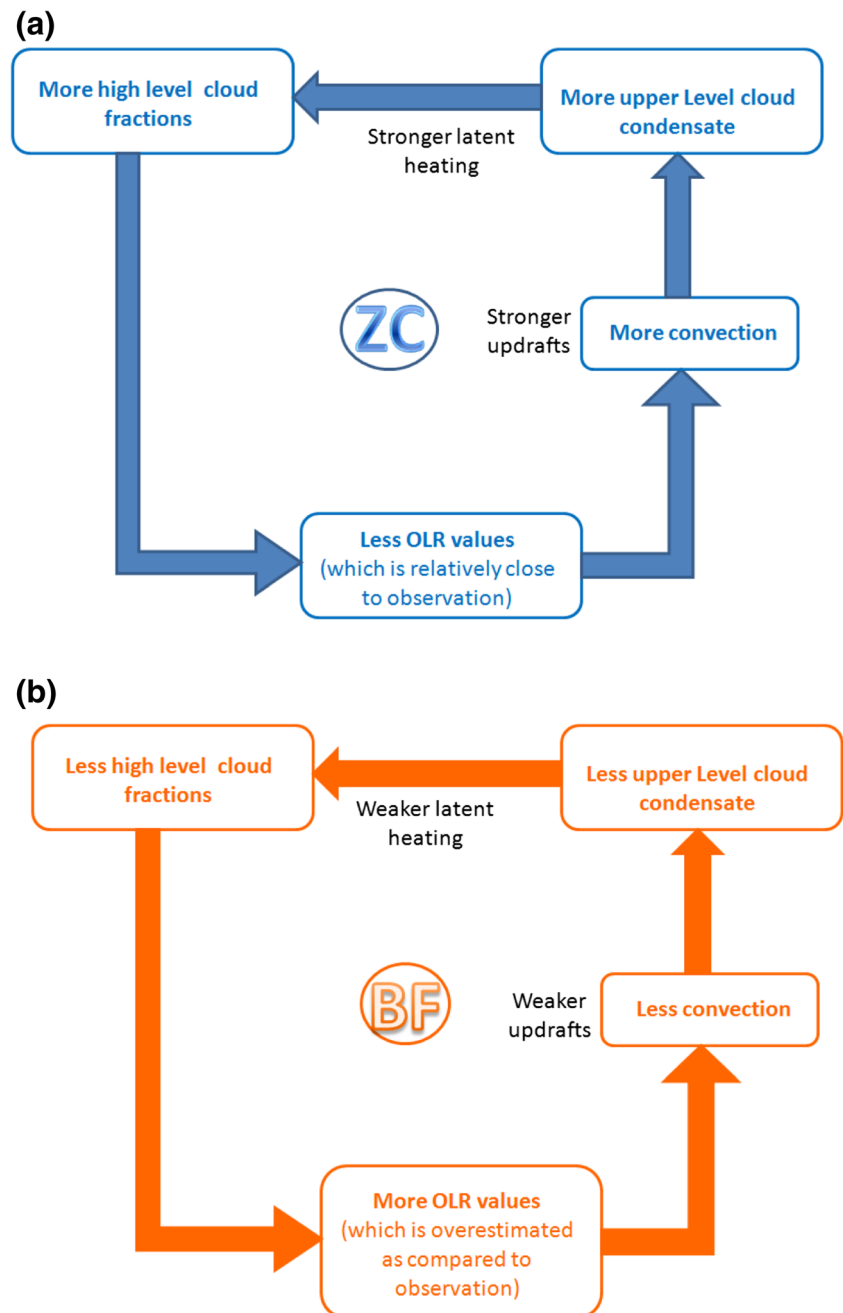


**Fig. 13** CFSv2-simulated JJAS OLR climatology ( $W/m^2$ ) for **a** ZC90, **b** BF90, **c** ZC95, and **d** BF95. Corresponding NOAA interpolated OLR is also presented (**e**)



**Fig. 14** The interaction among microphysics, thermodynamics, and dynamics works in tandem through a closed feedback loop which is represented by schematic diagram for **a** ZC and **b** BF



high-level cloud fraction in ZC schemes, and it will give feedback to OLR making them relatively low. As a result, ZC-simulated ISM is in relatively better agreement with observation. Result pinpoints that ZC scheme may be useful for the operational forecast of ISMR.

Further in-depth studies are required for the incorporation of realistic representation of cloud condensate for tackling the challenging problem of ISM through microphysics aspect. We believe that these future improvements

in representation of cloud condensate will lead to betterment of cloud fractions and realistic representation of latent heating/cooling, which, in turn, will give feedbacks to dynamics through convection.

**Acknowledgments** The authors acknowledge the support from Dr. Rajeevan, Director, IITM, and Dr. Suryachandra Rao, Chief Program Scientist, IITM, for pursuing the research. Ferret and NCL Freeware are used extensively in plotting. IBM High Power Computing (HPC) System, Prithvi facility is also acknowledged.

## References

- Adler RF, Huffman GJ, Chang A, Ferraro R, Xie P, Janowiak J, Rudolf B, Schneider U, Curtis S, Bolvin D, Gruber A, Susskind J, Arkin P, Nelkin E (2003) The version 2 global precipitation climatology project (GPCP) monthly precipitation analysis (1979-present). *J Hydro Meteorol* 4:1147–1167
- Arakawa A, Schubert WH (1974) Interaction of a cumulus ensemble with the large-scale environment, part 1. *J Atmos Sci* 31:674–701
- Baker MB (1997) Cloud microphysics and climate. *Science* 276:1072–1078
- Chaudhari HS, Shinde MA, Oh JH (2010) Understanding of anomalous Indian summer monsoon rainfall of 2002 and 1994. *Quat Int* 213: 20–32
- Chaudhari HS, Pokhrel S, Mohanty S, Saha SK (2013) Seasonal prediction of Indian summer monsoon in NCEP coupled and uncoupled model. *Theor Appl Climatol* 114:459–477
- Clough SA, Shephard MW, Mlawer EJ, Delamere JS, Iacono MJ, Cady-Pereira K, Boukabara S, Brown PD (2005) Atmospheric radiative transfer modeling: a summary of the AER codes. *J Quant Spectrosc Radiat Transf* 91:233–244
- De S, Hazra A, Chaudhari HS (2015) Does the modification in “critical relative humidity” of NCEP CFSv2 dictate Indian mean summer monsoon forecast?: Evaluation through thermodynamical and dynamical aspects. *Clim Dyn*. doi:10.1007/s00382-015-2640-z
- Delsole T, Shukla J (2010) Model fidelity versus skill in seasonal forecasting. *J Clim* 23:4794–4806
- Ek MB, Mitchell KE, Lin Y, Rogers E, Grunmann P, Koren V, Gayno G, Tarpley JD (2003) Implementation of Noah land surface model advances in the National Centers for Environmental Prediction operational mesoscale Eta model. *J Geophys Res* 1089(D22):8851. doi:10.1029/2002JD003296
- Ferrier BS, Lin Y, Black T, Rogers E, DiMego G (2002) Implementation of a new grid-scale cloud and precipitation scheme in the NCEP Eta model. Preprints, 15th Conf. on Numerical Weather Prediction, San Antonio, TX, Amer. Meteor. Soc., 280–283pp
- Griffies SM, Harrison MJ, Pacanowski RC, Rosati A (2004) A technical guide to MOM4, GFDL Ocean Group Technical Report, 5: 337 pp
- Hazra A, Chaudhari HS, Dhakate A (2015a) Evaluation of cloud properties in the NCEP CFSv2 model and its linkage with Indian summer monsoon. *Theor Appl Climatol*. doi:10.1007/s00704-015-1404-3
- Hazra A, Chaudhari HS, Rao SA, Goswami BN, Dhakate A, Pokhrel S, Saha SK (2015b) Impact of revised cloud microphysical scheme in CFSv2 on the simulation of the Indian summer monsoon. *Int J Climatol*. doi:10.1002/joc.4320
- Hazra A, Chaudhari HS, Pokhrel S (2014) Improvement in convective and stratiform rain fractions over the Indian region with introduction of new ice nucleation parameterization in ECHAM5. *Theor Appl Clim*. doi:10.1007/s00704-014-1163-6
- Hazra A, Goswami BN, Chen JP (2013a) Role of interactions between aerosol radiative effect, dynamics, and cloud microphysics on transitions of monsoon intraseasonal oscillations. *J Atmos Sci* 70:2073–2087
- Hazra A, Taraphdar S, Halder M, Pokhrel S, Chaudhari HS, Salunke K, Mukhopadhyay P, Rao SA (2013b) Indian summer monsoon drought 2009: role of aerosol and cloud microphysics. *Atmos Sci Lett* 14:181–186
- Hong S-Y, Pan H-L (1998) Convective trigger function for a mass-flux cumulus parameterization scheme. *Mon Weather Rev* 126:2599–2620
- Hu Y, Winker D, Vaughan M, Lin B, Omar A, Trepte C, Flittner D, Yang P, Nasiri SL, Baum B, Holz R, Sun W, Liu Z, Wang Z, Young, Stammes K, Huang J, Kuehn R (2009) CALIPSO/CALIOP cloud phase discrimination algorithms. *J Atmos Ocean Technol* 26:2293–2309
- Iacono MJ, Mlawer EJ, Clough SA, Morcrette J-J (2000) Impact of an improved longwave radiation model, RRTM, on the energy budget and thermodynamic properties of the NCAR Community Climate Model, CCM3. *J Geophys Res* 105:14873–14890
- Joseph PV, Sijikumar S (2004) Intraseasonal variability of the low level jetstream of Asian summer monsoon. *J Clim* 17:1449–1458
- Joseph PV, Sooraj KP, Babu CA, Sabin TP (2005). A cold pool in the Bay of Bengal and its interaction with the active-break cycle of the monsoon. *CLIVAR Exchanges* 34, 10(3), 10–12pp
- Kanamitsu M, Ebisuzaki W, Woollen J, Yang SK, Niilo J, Fiorino M, Potter GL (2002) NCEP–DOE AMIP-II Reanalysis (R-2). *Bull Am Meteorol Soc* 83:1631–1643
- Kim YJ, Arakawa A (1995) Improvement of orographic gravity wave parameterization using a meso-scale gravity wave model. *J Atmos Sci* 52:1875–1902
- Kripalani RH, Kulkarni A, Sabade SS, Khandekar ML (2003) Indian monsoon variability in a global warming scenario. *Nat Hazards* 29:189–206
- Kripalani RH, Singh SV, Arkin PA (1991) Large-scale features of rainfall and OLR over the Indian and adjoining regions. *Beitr Phys Atmosph* 64:159–168. **Contribution to Atmospheric Physics**
- Krishnamurti TN, Bedi HS, Subramaniam M (1989) The summer monsoon of 1987. *J Clim* 2:321–340
- Kulkarni A, Kripalani RH, Sabade SS (2010) Examining Indian monsoon variability in coupled climate model simulations and projections. *IITM Res Rep RR-125:1–34*
- Kumar S, Hazra A, Goswami BN (2014) Role of interaction between dynamics, thermodynamics and cloud microphysics on summer monsoon precipitating clouds over the Myanmar coast and the Western Ghats. *Clim Dyn* 43:911–924
- Liebmann B, Smith CA (1996) Description of a complete (interpolated) outgoing longwave radiation dataset. *Bull Am Meteorol Soc* 77: 1275–1277
- Lott F, Miller MJ (1997) A new subgrid scale orographic drag parameterization: its performance and testing. *Quart J R Meteorol Soc* 123: 101–127
- Misra V, Pantina P, Chan SC, DiNapoli S (2012) A comparative study of the Indian summer monsoon hydroclimate and its variations in three reanalyses. *Clim Dyn* 39:1149–1168
- Moorthi S, Pan HL, Caplan P (2001) NCEP operational MRF/AVN global analysis/forecast system. *NWS Technical Procedures Bulletin* 484: 14pp. Available at: <http://www.nws.noaa.gov>
- Moorthi S, Sun R, Xia H, Mechoso CR (2010) Low-cloud simulation in the Southeast Pacific in the NCEP GFS: role of vertical mixing and shallow convection. *NCEP Office Note* 463, 28 pp. Available online at: <http://www.emc.ncep.noaa.gov/officenotes/FullTOC.html#2000>
- Naidu CV, Krishna KM, Rao SR, Kumar OSRUB, Durgalakshmi K, Ramakrishna SSVS (2011) Variations of Indian summer monsoon rainfall induce the weakening of easterly jet stream in the warming environment? *Glob Planet Chang* 33:1017–1032
- Nakagawa M, Pan HL, Sun R, Moorthi S, Ferrier B (2011) Implementation of the Ferrier cloud microphysics scheme in the NCEP GFS. 24th Conference on Weather and Forecasting/20th Conference on Numerical Weather Prediction, Seattle, WA
- Pokhrel S, Rahaman H, Parekh A, Saha SK, Dhakate A, Chaudhari HS, Gairola RM (2012) Evaporation-precipitation variability over Indian Ocean and its assessment in NCEP Climate Forecast System (CFSv2). *Clim Dyn* 39:2585–2608
- Rajeevan M, Rohini P, Niranjana Kumar K, Srinivasan J, Unnikrishnan CK (2013) A study of vertical cloud structure of the Indian summer monsoon using CloudSat data. *Clim Dyn* 40:637–650
- Rao RR, Girish Kumar MS, Ravichandran M, Samala BK (2006) Observed mini-cold pool off the southern tip of India and its intrusion into the south central Bay of Bengal during summer monsoon season. *L06607*, doi:10.1029/2005GL025382

- Rienecker MM, Suarez MJ, Gelaro R, Todling R, Bacmeister J, Liu E, Bosilovich MG, Schubert SD, Takacs L, Kim GK, Bloom S, Chen J, Collins D, Conaty A, da Silva A, Gu W, Joiner J, Koster RD, Lucchesi R, Molod A, Owens T, Pawson S, Pegion P, Redder CR, Reichle R, Robertson FR, Ruddick AG, Sienkiewicz M, Woollen J (2011) MERRA: NASA's modern-era retrospective analysis for research and applications. *J Clim* 24:3624–3648. doi:10.1175/JCLI-D-11-00015.1
- Saha S, Moorthi S, Pan H-L, Wu X, Wang J, Nadiga S, Tripp P, Kistler R, Woollen J, Behringer D, Liu H, Stokes D, Grumbine R, Gayno G, Wang J, Hou YT, Chuang HY, Juang H-MH, Sela J, Iredell M, Treadon R, Kleist D, Delst PV, Keyser D, Derber J, Ek M, Meng J, Wei H, Yang R, Lord S, Dool HVD, Kumar A, Wang W, Long C, Chelliah M, Xue Y, Huang B, Schemm JK, Ebisuzaki W, Lin R, Xie P, Chen M, Zhou S, Higgins W, Zou CZ, Liu Q, Chen Y, Han Y, Cucurull L, Reynolds RW, Rutledge G, Goldberg M (2010) The NCEP climate forecast system reanalysis. *Bull Am Meteorol Soc* 91:1015–1057
- Saha SK, Pokhrel S, Chaudhari HS (2013) Influence of Eurasian snow on Indian summer monsoon in NCEP CFSv2 free run. *Clim Dyn* 41: 1801–1815
- Saha S, Moorthi S, Wu X, Wang J, Nadiga S, Tripp P, Behringer D, Hou Y-T, Chuang H-Y, Iredell M, Ek M, Meng J, Yang R, Mendez MP, van den Dool H, Zhang Q, Wang W, Chen M, Becker E (2014a) The NCEP Climate Forecast System Version 2. *J Clim* 27:2185–2208
- Saha SK, Pokhrel S, Chaudhari HS, Dhakate A, Shewale S, SabeerAli CT, Salunke K, Hazra A, Mahapatra S, Rao AS (2014b) Improved simulation of Indian summer monsoon in latest NCEP climate forecast system (CFSv2) free run. *Int J Climatol* 34:1628–1641
- Sanderson BM, Shell KM, Ingram W (2010) Climate feedbacks determined using radiative kernels in a multi-thousand member ensemble of AOGCMs. *Clim Dyn* 35:1219–1236
- Slingo A, Wilderspin RC, Brentnall SJ (1987) Simulation of the diurnal cycle of outgoing longwave radiation with an atmospheric GCM. *Mon Weather Rev* 115:1451–1457
- Stephens GL, Vane DG, Boain RJ, Mace GG, Sassen K, Wang Z, Illingworth AJ, O'Connor EJ, Rossow WB, Durden SL, Miller SD, Austin RT, Benedetti A, Mitrescu C (2002) The Cloudsat mission and A-train: a new dimension of space based observations of clouds and precipitation. *Bull Am Meteorol Soc* 83:1771–1790
- Sun R, Moorthi S, Mechoso CR (2010) Simulation of low clouds in the Southeast Pacific by the NCEP GFS: sensitivity to vertical mixing. *Atmos Chem Phys* 10:12261–12272
- Sundqvist H, Berge E, Kristjansson JE (1989) Condensation and cloud studies with mesoscale numerical weather prediction model. *Mon Weather Rev* 117:1641–1757
- Tao W-K, Simpson J, Lang S, McCumber M, Adler R, Penc R (1990) An algorithm to estimate the heat budget from vertical hydrometeor profile. *J Appl Meteorol* 29:1232–1244
- Thorsen TJ, Fu Q, Comstock J (2011) Comparison of the CALIPSO satellite and ground-based observations of cirrus clouds at the ARM TWP sites. *J Geophys Res* 116:D21203. doi:10.1029/2011JD015970
- Thompson A, Stefanova L, Krishnamurti TN (2008) Baroclinic splitting of jets. *Meteorol Atmos Phys* 100:257–274
- Trenberth KE, Guillemot CJ (1998) Evaluation of the atmospheric moisture and hydrological cycle in the NCEP/NCAR reanalyses. *Clim Dyn* 14:213–231
- Walcek CJ (1994) Cloud cover and its relationship to relative humidity during spring time midlatitude cyclone. *Mon Weather Rev* 122: 1021–1035
- Waliser DE, Li J-L, Woods CP, Austin RT, Bacmeister J, Chern J, Del Genio A, Jiang JH, Kuang Z, Meng H, Minnis P, Platnick S, Rossow WB, Stephens GL, Sun-Mack S, Tao W-K, Tompkins AM, Vane DG, Walker C, Wu D (2009) Cloud ice: a climate model challenge with signs and expectations of progress. *J Geophys Res* 114: 10.1029/2008JD010015
- Webster PJ, Magana VO, Palmer TN, Shukla J, Tomas RA, Yanai M, Yasunari T (1998) Monsoons: processes, predictability and the prospectus for prediction. *J Geophys Res* 103:14451–14510
- Winker DM, Vaughan MA, Omar A, Hu Y, Powell KA, Liu Z, Hunt WH, Young SH (2009) Overview of the CALIPSO mission and CALIOP data processing algorithms. *J Atmos Ocean Technol* 26:2310–2323
- Wu X, Moorthi KS, Okamoto K, Pan HL (2005) Sea ice impacts on GFS forecasts at high latitudes. In: Eighth conference on polar meteorology and oceanography, American Meteorological Society, San Diego, CA
- Xu KM, Randall DA (1996) A semiempirical cloudiness parameterization for use in climate models. *J Atmos Sci* 53:3084–3102
- Zhao QY, Carr FH (1997) A prognostic cloud scheme for operational NWP models. *Mon Weather Rev* 125:1931–1953